L-subshell ionization by proton and alpha-particle bombardment of Ta, Au, and Bi†

C. N. Chang, J. F. Morgan,* and S. L. Blatt
Department of Physics, The Ohio State University, Columbus, Ohio 43210
(Received 11 September 1974)

Cross sections for ionization of the L_{I}, L_{II}, and L_{III} subshells in Ta, Au, and Bi have been measured for proton energies from 1.0 to 5.5 MeV and α-particle energies from 1.0 to 11.0 MeV. X-ray spectra recorded with a Si(Li) detector were used to deduce the subshell ionization cross sections: $L\alpha$ components give L_{III} subshell ionization cross sections σ_{L_3}, and $L\gamma$ components were computer analyzed into $L\gamma_5$, $L\gamma_1$, $L\gamma_{2+3}$, and $L\gamma_4$ to give the L_{II} and L_{I} subshell ionization cross sections, σ_{L_2} and σ_{L_1}, respectively. The data are compared with simple model calculations. The necessity of including some small but significant additional effects in the plane-wave Born-approximation treatment, particularly wave functions more realistic than the normally assumed hydrogenic forms, is discussed.

I. INTRODUCTION

In the past several years a wealth of information has been published on K-shell ionization cross sections for positively charged particles. Recently, similar data have begun to be available on the L-shell ionization cross sections. Although the earliest data[1,2] were for total L-shell cross sections, with the advent of higher-resolution Si(Li) detectors, and the use of spectrum stripping techniques, it has become feasible to measure the ionization cross sections for the individual L subshells. The first published work on L-shell cross sections measured in this manner was the work of Datz *et al.*,[3] who studied L-shell cross sections for protons and alpha particles incident on gold.

The main thrust of K-shell ionization studies has been to understand the mechanism producing the inner-shell ionization. Three theories have been used to describe the mechanism for the production of inner-shell holes; the plane-wave Born approximation (PWBA),[4,5] the semiclassical approximation (SCA),[6,7] and the binary-encounter approximation (BEA).[8,9] One finds, in general, good agreement between total K-shell ionization cross sections and calculations based on these theories, even with the use of rather simple hydrogenic wave functions to describe the bound electrons.

As the cross-section measurements increase in precision and the theoretical understanding of the collision mechanism advances, it becomes feasible to study finer details of the processes and gain new physical insights. On the theoretical side, some efforts have been made to work out ionization cross sections in a distorted-wave Born approximation (DWBA), using Coulomb wave functions.[10] The evaluation of the atomic form factor with fairly sophisticated Hartree-Fock-Slater-type wave functions has become practical[10] with the advent of fast computing techniques. The improvements that arise from the use of better atomic wave functions in calculating inner-shell ionization processes are expected to be more pronounced for L-shell ionization than for collisions with K-shell electrons, especially the ionization of the $2s_{1/2}$ subshell.

Senashenko *et al.*[11] have used a nonrelativistic Born approximation with Coulomb wave functions for initial and final states of the electron to determine the theoretical dependence of ionization cross sections on the structure of the electron initial state. They showed that at an equal binding energy the momentum distribution of the $2s$ electron, $p^2|\phi_{2s}(p)|^2$, has larger values than that of the $1s$ electron, $p^2|\phi_{1s}(p)|^2$, at $p > 3p_0 Z_2/n$; while at $p \simeq p_0 Z_2/n$, the $1s$ is larger than the $2s$ (Fig. 1). [Here, $p_0 = \mu e^2/\hbar$, where μ is the reduced mass of the atomic system, i.e., $\mu \simeq m_e$ (the electron mass) for a heavy element; Z_2 is the charge of the target nucleus; and n is the principal quantum number of the electron bound states.]

A node exists in the wave function for the $2s$ state in the vicinity of $p = p_0 Z_2/n$. All these differences between the $2s$ and $1s$ wave functions predict different projectile energy dependences for the ionization cross sections of $2s$ and $1s$ states.[11] Since the radial dependence of the $2p$ states is very similar to that of the $1s$ state (which has no node in its wave function either in coordinate representation or momentum representation, except at the origin), the study of the ionization of $2p$ and $2s$ states would be very instructive and provide a fairly direct measure of some nontrivial features of the atomic states, including the extent to which hydrogenic wave functions are capable of describing them.

In this paper, we report measurements of the L-subshell ionization cross sections of elements ranging from $Z_2 = 73$ (Ta) to $Z_2 = 83$ (Bi), induced by proton and alpha-particle impact in the energy range where the $2s$ cross section differs most noticeably from the $2p$. Comparisons of these cross sections with calculations based on the three

models for inner-shell ionization are also presented.

II. EXPERIMENTAL METHOD

The Ohio State University 5.5-MV Van de Graaff accelerator was used to produce proton beams from 1.0 to 5.5 MeV and alpha-particle beams from 1.0 to 11.0 MeV. Doubly ionized alpha particles were used in the energy range from 5.0 to 11.0 MeV. A check was made to assess the possible ion-source contamination of H_2^+, which would affect the results in He^{++} runs. Both singly and doubly ionized alpha particles were run at 5.0 MeV, and the $L\alpha$ x-ray yield with each beam was the same within experimental uncertainties.

The target chamber contained a beam collimator and a surface-barrier detector used as a beam and target monitor. The target was oriented at 45° relative to the beam line so that the upward-looking Si(Li) detector can get an unobstructed view of the beam spot. Two suppressor rings were installed on the ends of the beam collimator to suppress the secondary electrons from it, so that this system can be used when a thick target is bombarded. This also eliminates secondary-electron bombardment of the target, even though its influence on the cross-section measurement is expected to be negligible.[12] In order to let the low-energy photons (≤100 keV) get out of the chamber, a $\frac{3}{8}$-in.-diam $\times 10^{-3}$-in.-thick mylar window was installed.

Protons were detected with a KeveX model 3000 Si(Li) detector. It was necessary to keep the count rate under 4000 counts/sec to minimize the pileup distortion of the very long detector pulses; in order to allow the use of beam currents high enough for accurate integration, the detector solid angle was kept small. Beam currents were varied between 5 and 40 nA, depending on cross section, in order not to require any change in the detector-target distance. Typical L x-ray spectra for tantalum, gold, and bismuth are shown in Fig. 2. They are produced by 4.5-MeV proton bombardment with beam current ≃10 nA, and count rate ≃300 counts/sec. The $L\gamma$ x-ray complex was resolved by a Gaussian fitting routine, and the counts of $L\gamma_1 + L\gamma_5$ and $L\gamma_2 + L\gamma_3 + L\gamma_4$ were obtained (see below). Small amounts of the tantalum L x-ray lines are also observed in the gold and bismuth runs, as shown in Fig. 2. This comes from the tantalum target frame. This source of background does not have any effect on the measurements of the $L\gamma$ x-rays of Au and Bi, since their peak positions are outside those of the tantalum L x-ray group. The problem was eliminated with the tantalum target by using a different target frame.

Targets used in the experiment were thin foils (all ≲100 $\mu g/cm^2$) evaporated on thin (10 $\mu g/cm^2$) carbon backings. Target thicknesses were measured in a subsidiary experiment by bombarding with 3.0-MeV protons and assuming the cross sec-

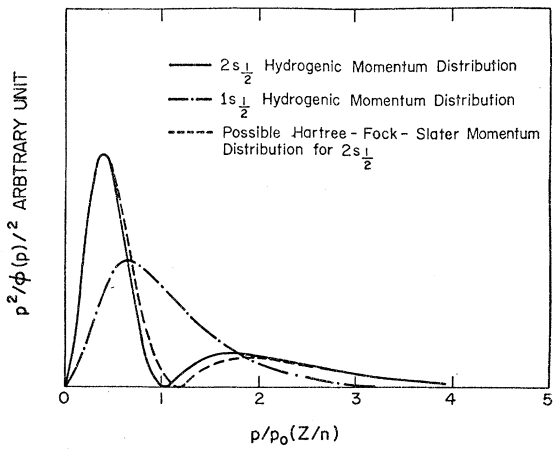

FIG. 1. Hydrogenic momentum distributions of 1s and 2s electrons with equal binding energy.

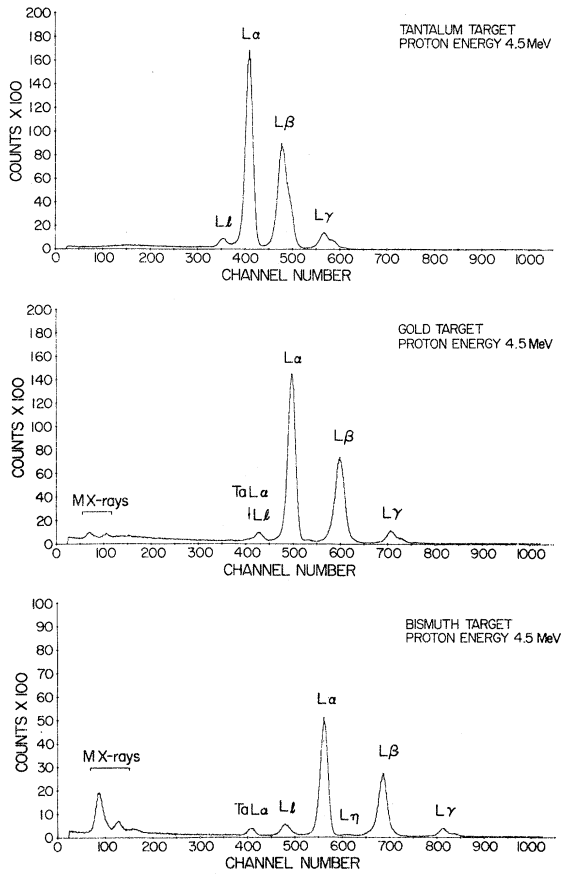

FIG. 2. L x-ray spectra of Ta, Au, and Bi induced by 4.5-MeV incident protons.

tion at forward angles was well described by the Rutherford formula. The solid angles for the detectors used in this measurement have been carefully studied in this laboratory.[13] This measurement gives target thicknesses with an uncertainty of ±2%. As mentioned above, a separate detector was used to constantly monitor the target thickness and beam spot position during the x-ray runs. This proved invaluable for the bismuth target, since its low melting point (~271 °C) caused some target deterioration under conditions of high beam currents, especially for alpha beams. Corrections for this target-thickness change never amount to more than 10%.

The efficiency of the Si(Li) detector was calibrated by replacing the target in vacuo with a series of calibrated sources, the rest of the chamber-detector geometry remaining exactly the same as during the experimental runs. A typical detector efficiency for the tantalum $L\gamma$ group, including the solid-angle factor, was found to be 1.36×10^{-4}.

III. DATA REDUCTION AND RESULTS

A. Data analysis

The production cross sections for each component of the L x-rays (Fig. 2) can be easily obtained by the equation

$$\sigma^x_{Ly} = Y_{Ly}/I\epsilon T ,$$

where Y_{Ly} is the x-ray yield of one of the L x-ray components Ly for a given number of incident particles on the target, I. (The index y refers to a particular component of the L x-rays such as l, α, β, γ, etc.) The term ϵ represents the over-all efficiency of the Si(Li) detector (including its solid angle and corrections for all absorbers in the path through which the photons travel from the target to the detector) and T is the target thickness actually seen by the beam.

In order to interpret the measured x-ray production cross sections one has to relate them to the theoretical total ionization cross sections. Because of the complicated decay scheme of the L x-rays and the difficulties involved in resolving all the L x-ray lines (especially the $L\beta$ group, which contains contributions from all L subshells), one usually evaluates the individual x-ray production cross section for each resolved component and runs through the following analytic formulas to relate the x-ray production cross sections to the ionization cross sections:

$$\sigma^x_{Ll} = (\sigma_{L_1}f_{13} + \sigma_{L_1}f_{12}f_{23} + \sigma_{L_2}f_{23} + \sigma_{L_3})\omega_3 F_{3l} , \quad (1a)$$

$$\sigma^x_{L\alpha} = (\sigma_{L_1}f_{13} + \sigma_{L_1}f_{12}f_{23} + \sigma_{L_2}f_{23} + \sigma_{L_3})\omega_3 F_{3\alpha} , \quad (1b)$$

$$\sigma^x_{L\beta} = \sigma_{L_1}\omega_1 F_{1\beta} + (\sigma_{L_1}f_{12} + \sigma_{L_2})\omega_2 F_{2\beta} + (\sigma_{L_1}f_{13} + \sigma_{L_1}f_{12}f_{23} + \sigma_{L_2}f_{23} + \sigma_{L_3})\omega_3 F_{3\beta} , \quad (1c)$$

and

$$\sigma^x_{L\gamma} = \sigma_{L_1}\omega_1 F_{1\gamma} + (\sigma_{L_1}f_{12} + \sigma_{L_2})\omega_2 F_{2\gamma} , \quad (1d)$$

where σ^x_{Ll}, $\sigma^x_{L\alpha}$, $\sigma^x_{L\beta}$, and $\sigma^x_{L\gamma}$ are the x-ray production cross sections of the components Ll, $L\alpha$, $L\beta$, and $L\gamma$; σ_{L_1}, σ_{L_2}, and σ_{L_3} are ionization cross sections of the subshells $L_{\rm I}$, $L_{\rm II}$, and $L_{\rm III}$, respectively; ω_1, ω_2, and ω_3 are the subshell fluorescence yields; F_{ny} (F_{3l}, $F_{3\alpha}$, $F_{3\beta}$, ..., etc.) are the fraction of the radiation width of the subshell L_n($L_{\rm I}$, $L_{\rm II}$, and $L_{\rm III}$) contained in the yth spectral line, i.e.,

$$F_{ny} = \Gamma_{ny}/\Gamma_n$$

(for example, $F_{3l} = \Gamma_{3l}/\Gamma_3$), where Γ_n is the total radiative width of L_n. The parameters f_{12}, f_{23}, and f_{13} are the Coster-Kronig transition probabilities $L_{\rm I} \rightarrow L_{\rm II}$, $L_{\rm II} \rightarrow L_{\rm III}$, and $L_{\rm I} \rightarrow L_{\rm III}$, respectively (the arrow indicates the direction of the electron-vacancy transition between subshells).

Most of the previous work done on the L subshell[14,15] used theoretical values of σ_{L_1}, σ_{L_2}, and σ_{L_3} combined with known ω's, F's, and f's on the right-hand side of the Eq. (1) to evaluate the x-ray production cross section on the left-hand side for comparisons with experiment. The advantage of this procedure is that it may get rid of the Coulomb deflection effect and some of the distortions of L-subshell electron wave functions due to the incoming charged particles, in cases where only ratios of the L x-ray production cross sections are to be compared. This serves as a comparison between experiment and theory for a particular correction in the interaction mechanism (cf. Ref. 14, which investigates the relativistic correction in PWBA). However, the actual features of the individual ionization cross sections may be hidden in this way. For the purpose of obtaining actual ionization cross sections from L x-ray measurements, we selected the $L\alpha$ and $L\gamma$ x-rays to do a detailed analysis; the use of such an analysis is explained below.

The barely resolved $L\gamma$ x-rays have been computer analyzed into four Gaussians with over-all shape fits having χ^2, per degree of freedom, values of around 1.2 ± 0.5. Four components of $L\gamma$ were obtained: $L\gamma_5$ and $L\gamma_1$, which are related to the $L_{\rm II}$ subshell; and $L\gamma_{2+3}$ and $L\gamma_4$, which are related to the $L_{\rm I}$ subshell. Examples of this fitting for Ta, Au, and Bi are presented in Fig. 3. The peak energies are indicated by the arrows, and agree excellently with values measured in high-resolution

experiments.

Equation (1d) can be broken into

$$\sigma^x_{L\gamma_{2+3}} + \sigma^x_{L\gamma_4} = \sigma_{L_1}\omega_1 F_{1\gamma_{2+3+4}} \quad (2)$$

and

$$\sigma^x_{L\gamma_5} + \sigma^x_{L\gamma_1} = (\sigma_{L_1} f_{12} + \sigma_{L_2})\omega_2 F_{2\gamma_{5+1}} . \quad (3)$$

The unresolvable $L\gamma_6$ in $L\gamma_{2+3}$ (see Fig. 3) may raise a significant error in deducing σ_{L_1} from the uncorrected x-ray production cross sections. This problem can be overcome by an iterative procedure, first estimating σ_{L_2} and σ_{L_1} from Eq. (3) and Eq. (1d) by ignoring f_{12} in the first place as described in Ref. 24. This problem was also discussed in Ref. 3. The calculations can be iterated until consistency of σ_{L_1} is reached. In our data analysis, one iteration is good enough to give consistency within 0.01%.

σ_{L_3} was obtained through Eq. (1b) by using the measured $L\alpha$ x-ray production cross sections $\sigma^x_{L\alpha}$, and $\sigma_{L_1}, \sigma_{L_2}$, which were deduced as described in the last paragraph. A consistency check was also made (for each element) for the $L\beta$ group through the comparison between the measured $\sigma^x_{L\beta}$ and that calculated from Eq. (1c) by using our deduced values of σ_{L_1}, σ_{L_2}, and σ_{L_3}. The measured values for the $L\beta$ yields in Ta and Au are systematically some 4% higher than those calculated from Eq. (1c), which could be due to uncertainties in the efficiency calibration of the detector in the interpolated region.

B. Atomic parameters

The uncertainties in converting x-ray production cross sections into ionization cross sections depend mostly on the accuracy of the fluorescence yields ω_1, ω_2, and ω_3, and the fractional probabilities f_{12}, f_{23}, and f_{13}.

The fractional widths used here are taken from the radiative emission rates calculated by Scofield.[16] Recently observed $L\alpha/Ll$ ratios, both in a source experiment[17] and in a particle-induced measurement,[15] have shown some discrepancies from Scofield's calculation. In the source experiment, covering a range of atomic numbers $55 \leq Z \leq 94$, the theoretical ratios are found to be underestimated at low Z ($Z \leq 73$), while in the particle experiments, the theoretical ratios are higher for Sm ($Z = 52$). The lower experimental ratios of $L\alpha/Ll$ observed for Sm may be due to some multi-ionization occurring in L_{III} and $M_{IV,V}$ for $L\alpha$. We thus checked our Ta $L\alpha/Ll$ data at several energies; good agreement was obtained with Scofield's value. Other experiments[18,19] also show that Scofield's values are quite good for the high-Z region. We evaluated some of the partial radiation widths $F_{n\gamma}$ from the experimental values available in Ref. 18 to compare with Scofield's values. We found that there is a good agreement between theory and experiment. Therefore, in our converting process, we use Scofield's values for all the elements Ta, Au, and Bi (Pb values in Scofield were used for Bi owing to lack of Bi values).

A review article of Bambynek *et al.*[20] on fluorescence yields and Coster-Kronig transition probabilities, which reviewed this field up to 1972, was strongly relied on to obtain values of these quantities. Both experimental and theoretical values of these quantities for Ta, Au, and Bi are given in Table I. Here the "references" are listed in Ref. 20, and ν_1, ν_2, and ν_3 are Coster-Kronig–corrected fluorescence yields, defined as

$$\sigma^x_L = \nu_1\sigma_{L_1} + \nu_2\sigma_{L_2} + \nu_3\sigma_{L_3} ,$$

and have the relations

$$\nu_1 = \omega_1 + \omega_2 f_{12} + \omega_3(f_{13} + f_{12}f_{23}) , \quad (4)$$

$$\nu_2 = \omega_2 + \omega_3 f_{23} , \quad (5)$$

$$\nu_3 = \omega_3 . \quad (6)$$

The values we used in converting x-ray production cross sections to ionization cross sections are shown underlined. Tungsten theoretical values are tabulated as an approximation for Ta. The value $\omega_1 = 0.096$, for Ta, was calculated by putting experimental values of ν_1 (=0.218), ν_2 (=0.303),

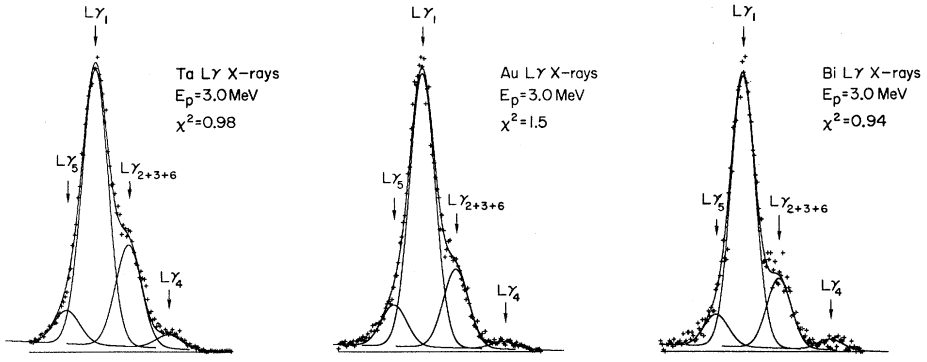

FIG. 3. Gaussian fits to the $L\gamma$ x-ray spectra of Ta, Au, and Bi. The centroids of the four Gaussians and the χ-square values are indicated.

TABLE I. Fluorescence yields and Coster-Kronig transition probabilities of Ta, Au, and Bi. (Values used in converting x-ray production cross sections to ionization cross sections are shown underlined.)

	ω_1	ω_2	ω_3	ν_1	ν_2	f_{12}	f_{13}	f_{23}	Ref. [b]
Ta		0.25 ± 0.02	0.27 ± 0.01		0.31 ± 0.01			0.020 ± 0.04	Rao (1965b)
(Expt.)			0.25 ± 0.103		0.37 ± 0.06				Jopson (1964a)
			0.191	0.284	0.326				Kustner (1935)
	0.096[a]	0.257 ± 0.013	0.228 ± 0.013	0.218 ± 0.016	0.303	<0.14	<0.36	0.148 ± 0.010	Mohan (1970a)
		(0.269)[a]			(0.303)	(0.160)	(0.324)		
			0.254 ± 0.025		0.303 ± 0.030				Price (1968)
							0.19		Ferreira (1965)
				0.22 ± 0.01					Rao (1966)
W	0.115	0.287	0.268			0.195	0.332	0.123	McGuire (1971a)
(Theo.)	0.138	0.271	0.253			0.160	0.324	0.117	Chen (1971a) and Crasemann (1971)
Au	0.210[a]	0.236[a]	0.276	0.410	0.272	(0.083)	(0.644)	(0.132)	Kustner (1935)
(Expt.)	0.201[a]	0.211[a]				(0.25)	(0.51)	(0.22)	
			0.31 ± 0.04						Jopson (1964a)
	0.173[a]	0.253[a]	0.317 ± 0.025	(0.410)	0.395 ± 0.032	(0.083)	(0.644)	(0.132)	Price (1968)
	0.150[a]	0.325[a]	(0.317)	(0.410)	(0.395)	0.25 ± 0.13	0.51 ± 0.13	(0.22)	Paschke (1963)
							0.61 ± 0.07		Ferreira (1965)
(Theo.)	0.105	0.357	0.327			0.083	0.644	0.132	McGuire (1970a)
Bi			0.367						Kustner (1935)
(Expt.)			0.36						Risch (1958)
						0.19 ± 0.05	0.58 ± 0.05	$0.06^{+0.14}_{-0.06}$	Ross (1955)
						0.18 ± 0.02	0.58 ± 0.02	(0.164)	Freund and Fink (1969)
					0.51 ± 0.08				Jopson (1964a)
					0.41 ± 0.039				Price (1968)
(Theo.)	0.120	0.417	0.389			0.069	0.656	0.101	McGuire (1970a)

[a] Calculated values from existing data combined with other values from other sources which are indicated in parentheses.

[b] Listed in Ref. 20.

ω_3 (=0.228), and f_{23} (=0.148), and theoretical values of f_{12} (=0.160) and f_{13} (=0.324) into Eqs. (4) and (5). This value was used instead of McGuire's value, $\omega_1 = 0.115$, to do the conversion.

C. Results and error analysis

The ionization cross sections $\sigma_{L_1}, \sigma_{L_2}, \sigma_{L_3}$ for the various elements, obtained as described in Secs. III A and III B, are shown in Figs. 4–6 together with various theoretical calculations to be discussed below. Tabulated values of the cross sections are available from the authors.

The standard counting errors for the $L\alpha$ x-rays of Ta, Au, and Bi induced by proton bombardment are less than 1%; those for $L\gamma$ x-rays which relate to L_{I} ionization (i.e., $L\gamma_{2+3+4}$) are generally less than 10%, and are less than 6% for $L\gamma$ x rays which relate to L_{II} ionization (i.e., $L\gamma_{1+5}$), except where the incident-proton energy is below 2.0 MeV. For these low energies, 10–15% standard errors were estimated.

Aside from this uncertainty due to the statistics of the counting process, the other sources of experimental uncertainty come mainly from the measurements of target thickness and the efficiency of the Si(Li) detector. They contribute an over-all error of about 15%. The self-absorption by the target atoms was found to be less than 1%; corrections for this effect were not made to the data. The angular distributions were assumed to be isotropic on the basis of previously published data[21,22] and on the basis of angular momentum considerations.[23]

In the conversion process to ionization cross sections from x-ray yields, uncertainties in the atomic parameters, such as fluorescence yields, radiative transition rates, and Coster-Kronig

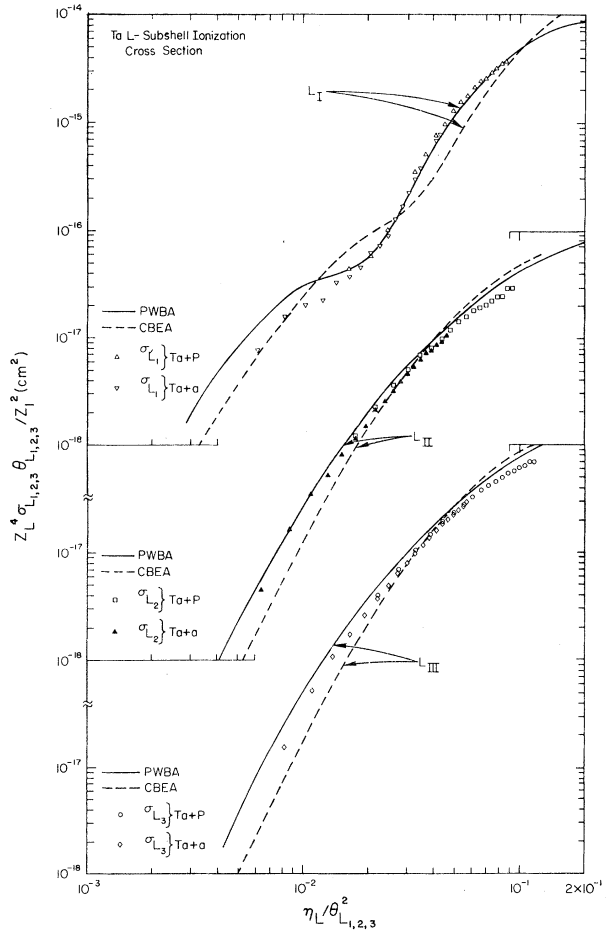

FIG. 4. L-subshell ionization cross sections for Ta, obtained from both proton and alpha-particle bombardment. Curves of the PWBA and BEA theories are shown for comparison. The statistical and absolute errors are discussed in the text.

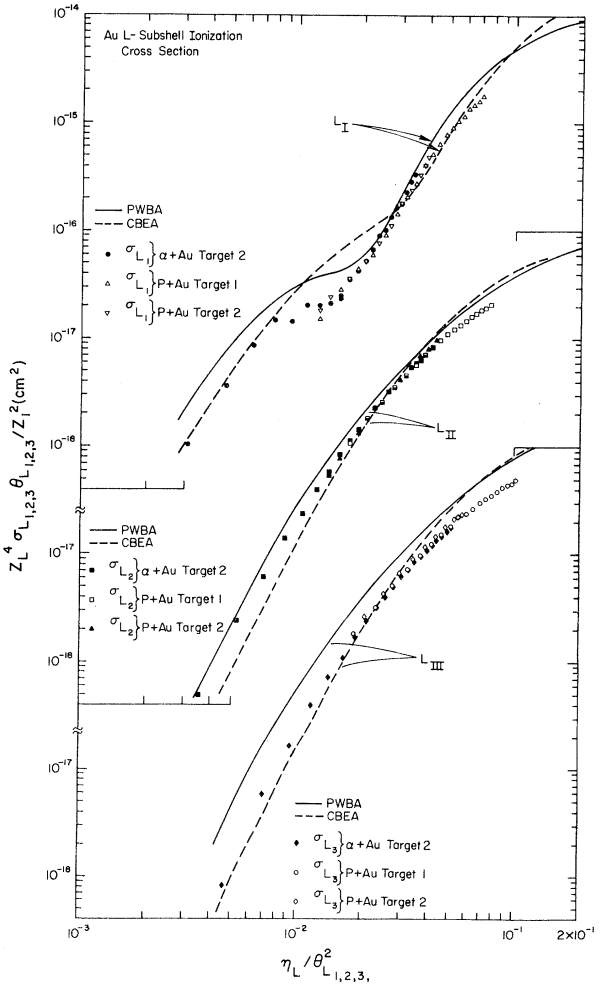

FIG. 5. Ionization cross sections for Au. See Fig. 4 caption for details.

transition probabilities, may increase the uncertainty of the final absolute ionization cross sections. Extensive discussion has been made in Ref. 24; the errors from this source could amount to a maximum of 14% for σ_{L_1} and σ_{L_3}, and $\simeq$21% for σ_{L_2}.

Including the above mentioned uncertainties from the measurements of the absolute yields of the components of the L x-rays ($L\gamma_{1+5}$ and $L\gamma_{2+3+4}$ $\simeq$15–18%, $L\alpha \simeq 15\%$), one finds that the *absolute* cross sections in this work are known to 21% for σ_{L_3}, 28% for σ_{L_2}, and 22% for σ_{L_1}. The *relative* uncertainties are close to the statistical errors, since the other factors such as target thickness, efficiency of the Si(Li) detector, and all the atomic parameters should affect the results uniformly.

IV. DISCUSSION

The resulting L-subshell ionization cross sections for Ta, Au, and Bi are plotted in Figs. 4–6. The gold data are in excellent agreement with the previous work of Datz *et al.*[3] Nonrelativistic PWBA and CBEA calculations are also included for comparison. The theoretical curves for PWBA are obtained from the listed values of $f(\Theta_{L_n}, \eta_L)$ calculated by Choi *et al.*,[25] and those of CBEA are obtained from scaling the cross sections which were calculated by Hansen,[9] using the appropriate hydrogenic momentum distribution for each L subshell. The choice of the units of the coordinates follows the PWBA theory, which predicts that at low bombarding energies, the cross sections follow, approximately, the scaling law

$$(Z_L^4 \sigma_{L_n} \Theta_{L_n})/Z_1^2 = f(\eta_L/\Theta_{L_n}^2) .$$

The parameters Z_L, Θ_{L_n}, and η_L are defined in Refs. 4 and 25. Z_L is the effective charge of the target nucleus, Θ_{L_n} is proportional to the ratio of the true binding energy of the L_n subshell to that predicted by a hydrogenic wave function, and η_L is proportional to the ratio of the incident energy to the average binding energy of L-shell electrons as predicted by hydrogenic wave functions.

The PWBA is seen to describe the observations much better than the CBEA, especially the energy dependence of the shape of each ionization cross section. The absolute values of the PWBA cross sections, however, overestimate the experimental results by upwards of four standard deviations, especially at low incident energies. Overestimated absolute values predicted by PWBA have been noticed for a long time in the study of K-shell ionization when the incident energy of the charged particle is low, i.e., when the criteria for the validity of PWBA are not met. Two main corrections have to be made: (i) the binding energy change correction and (ii) the Coulomb deflection effect. The criteria for these effects to be significant for K-shell ionization are discussed in detail by Basbas *et al.*,[26] who use perturbation theory to do a series expansion of the ionization cross section both in terms of the strength of the Coulomb interaction between the incident particle and the atomic nucleus, and in terms of the strength of the Coulomb interaction between the incident charged particle and the atomic electrons, and conclude as follows.

(i) Whenever

$$v/V_k \lesssim \Theta_k/2 \text{ (i.e., } \eta_k/\Theta_k^2 \lesssim \tfrac{1}{4}) , \qquad (7)$$

where v is the incident particle's velocity and V_k is the mean velocity of K-shell electrons, the binding-change effect is significant for K-shell ionization. This simply states that the K-shell wave functions will be distorted (the binding energy is increased) by the presence of the incident charged

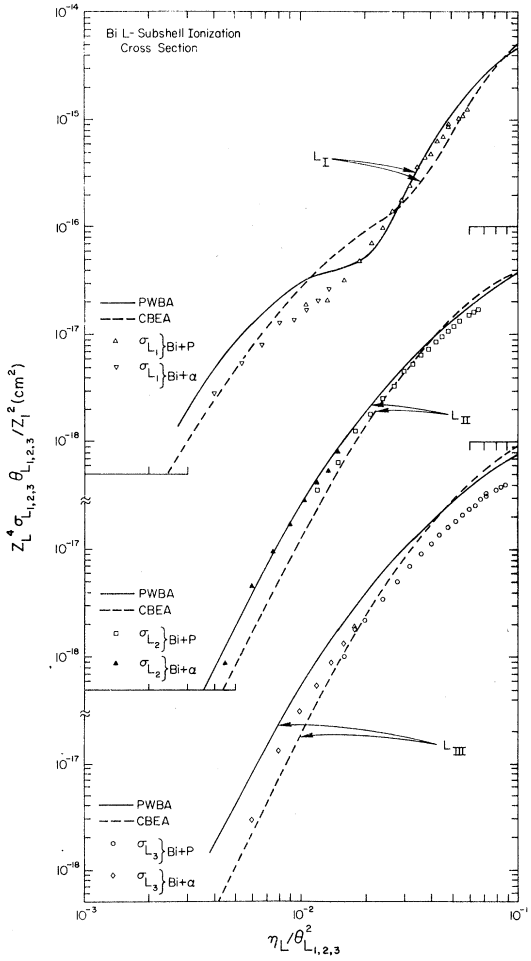

FIG. 6. Ionization cross sections for Bi. See Fig. 4 caption for details.

particle near the nucleus if the electron response time $1/\omega_k$ is comparable to the particle-electron interaction time $\simeq a_k/v$, where $a_k = a_0/Z_k$ and a_0 is the Bohr radius. Thus the probability of ionization will be decreased and the actual cross sections lower than the PWBA cross section.

(ii) Whenever

$$q_0^{-1} \leq \frac{Z_1 Z_2 e^2}{M_\mu V^2} \simeq Z_1 \left(\frac{m}{M_\mu}\right)\left(\frac{V_k}{v}\right)^2 a_k , \qquad (8)$$

the Coulomb deflection of the incident charged particle in the repulsive field of the target atomic nucleus must be significant and will affect the K-shell ionization cross sections. Here, q_0 is the minimum momentum transfer from the incident ion to the bound electron and is equal to the energy transferred to the electron (roughly equal to E_{binding}, since the outgoing electron kinetic-energy distribution very strongly favors very low energies) divided by $\hbar v$; m is the electron mass; and M_μ the reduced mass of the point charges $Z_1 e$ and $Z_2 e$ which undergo Coulomb interactions. The quantity $Z_1 Z_2 e^2/M_\mu V^2$ is equal to one-half of the distance of closest approach in a head-on collision in the Coulomb field of two point charges $Z_1 e$ and $Z_2 e$. The quantity q_0^{-1} is called the optimum penetration distance of the incident charged particle, since when the impact parameter is $\simeq q_0^{-1}$, the ionization probability is the greatest.[6] Therefore, Eq. (8) simply states the criterion for the optimum penetration distance being small compared to the distance of closest approach of these two point charged particles. Under this condition, one immediately sees that the incident charged particle will be deflected by the repulsive Coulomb field of the target atomic nucleus before reaching the position of maximum ionization probability, thus causing the actual cross section to fall below the PWBA calculation.

Applying these same criteria to the L shell, we notice that our energy range ($\eta_L \cong 0.002$–0.04, and $\eta_L/\Theta_L^2 \lesssim 0.1$) falls in a region where the corrections of the binding effect and the Coulomb-deflection effect are important. We have thus compared our Au data to calculations in the semiclassical approximation[7] (SCA) (Fig. 7). The SCA calculations include Coulomb deflection by considering the path of the projectile to be a hyperbola instead of a straight line, and show better agreement with the data for the L_{III}-subshell ionization cross sections, at incident energy per amu $\lesssim 2.0$ MeV for both proton and alpha-particle bombardments, than does the PWBA. For L_{II} ionization, the proton data below 2.0 MeV also follow SCA. Deviations from SCA in L_{II} are observed for alpha energies below 1.0 MeV/amu. The plot of $\sigma_{L_3}/\sigma_{L_2}$ ratios versus particle energies exhibits this feature in a more pronounced way (Fig. 10). We will discuss this deviation later. There are no SCA calculations available for Ta and Bi; however, from the results given above for gold, the Coulomb-deflection effect is clearly sizable and predictable when the incident-particle energy is below 2.0 MeV/amu. When the energy is above 2.0 MeV/amu the ionization cross sections of the L_{III} and L_{II} subshells are not well described by the SCA calculations.

There is no evidence that the ionization cross section of L_{I} is well predicted by either CBEA or SCA. The general shape of the L_{I} cross section follows PWBA reasonably well, in the sense that both data and predictions of PWBA tend to consist of two smooth increasing curves whose junction is around $\eta_L/\Theta_L^2 \simeq 0.01$. This not only strongly indicates that a quantum-mechanical treatment should be better than other approaches (e.g., SCA

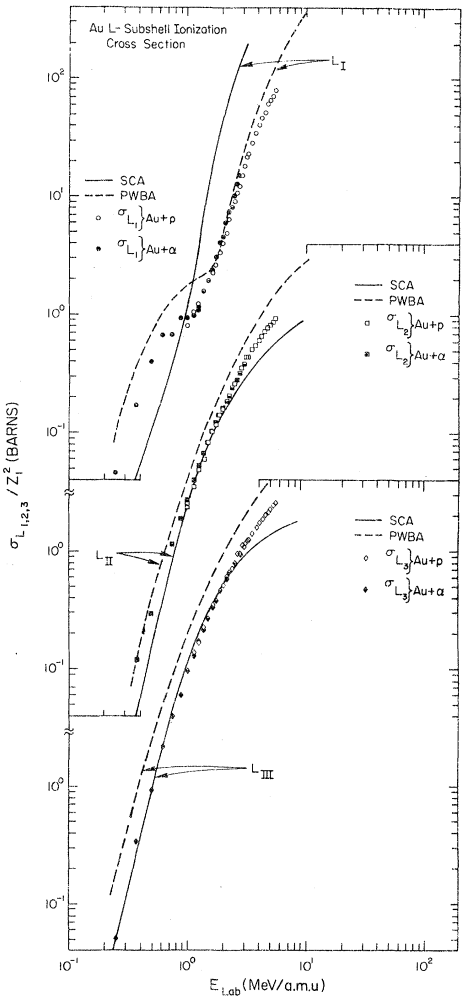

FIG. 7. Gold L-subshell ionization cross sections compared with PWBA and SCA theory.

and CBEA), but also shows clearly that there is a strong correlation between the incident energy of the charged particle and the momentum distribution of the bound electrons. The momentum distribution of the $2s_{1/2}$ electron has a node at $p=(Z_L/2a_0)\hbar$ according to calculations using nonrelativistic hydrogenic wave functions[11] (Fig. 1), while the momentum distributions of the $2p_{1/2}$ and $2p_{3/2}$ electrons are similar to that of $1s_{1/2}$ electrons, i.e., without nodes except at $p=0$. The gross behavior of $2p_{1/2}$ and $2p_{3/2}$ ionization thus is pretty much similar to that of $1s_{1/2}$ (K-shell) ionizations. The different form of the initial wave function of the $2s_{1/2}$ states from that of the p states produces the "kink" in the energy dependence of the ionization cross sections of the $L_{\rm I}$ subshell. Basing his considerations on PWBA and the node of the momentum distribution of a $2s_{1/2}$ electron at $p=(Z_L/2a_0)\hbar$, Merzbacher[27] has estimated roughly that the sharp change in the energy dependence of the cross section would be expected in the neighborhood of $\eta_L/\Theta_L^2 \simeq 0.06$. Experimentally this behavior was first reported by Datz *et al.*[3] in the $L_{\rm I}$ ionization cross section of gold. Qualitatively, both their data and ours are in good agreement with this prediction. The other noticeable correlation between the particle-energy dependence of the cross section and the electron-momentum distributions is that the ionization cross sections for the $L_{\rm I}$ subshell are much larger than those for the $L_{\rm II}$ subshell at an energy below $\eta_L/\Theta_L^2=0.01$, which corresponds to the larger amplitude of the momentum distribution of the $2s_{1/2}$ electrons in the higher-momentum region ($p \gtrsim 3p_0 Z/n$, Fig. 1). (This is a consequence of the optimum penetration distance being smaller, and thus sampling higher momentum components, for lower bombarding energies, within the energy range under consideration.) The two peaks of the momentum distribution of the $2s_{1/2}$ electron (Fig. 1) may thus contribute to the two smooth increasing curves seen in the energy dependence of the ionization cross section.

It is much easier to understand the correlations between the incident ion energy and the initial electron wave function from the semiclassical picture proposed by Bang and Hansteen.[6] By introducing the impact parameter b, Bang and Hansteen find that the ionization is most likely to occur at $b \simeq q_0^{-1}$ (q_0^{-1} is thus called the "optimum penetration distance"). If this optimum penetration distance corresponds to a place where the electron has the least amplitude in its momentum distribution [and according to the Bohr atomic picture, one can grossly estimate the place where the electron has the least chance to be, i.e., $r=\hbar/p$ and $p=(Z_L/2a_0)\hbar$], the ionization cross section must change around there. Therefore, the location of the kink in the energy-dependent ionization cross section could be estimated as

$$1/q_0 \simeq 2a_0/Z_L . \tag{9}$$

This immediately gives $\eta_L \simeq \Theta_L^2/2^4$, i.e., $\eta_L/\Theta_L^2 \simeq 0.06$. All the above discussions show that when the incident energy is decreasing, the momentum of the electrons which are most likely to be ionized is increasing, or vice versa. Apparently, in our energy range, the majority of the $2s_{1/2}$ electrons to be ionized fall in the vicinity of the node of the momentum distribution.

Qualitatively therefore, PWBA describes the $L_{\rm I}$ observations quite well. Quantitatively, substantial deviations between data and theory occur at energies near to and below the kink. There is a tendency for the upper smooth curve to extend downwards to the low-energy side of the position of the kink predicted by PWBA (i.e., the junction point of the two smooth curves in the data occurs at a lower energy than that of PWBA). This simply indicates that the node in the momentum distribution of the $2s_{1/2}$ electron must be at a higher momentum than is predicted by the nonrelativistic hydrogenic wave functions. This, in turn, implies that the nonrelativistic hydrogenic wave function used in PWBA is not adequate. In fact, for heavy atoms, a relativistic correction for the bound electrons has been found to be important.[28,14] The existing relativistic calculations were terminated at $\eta_L \simeq 0.01$; no calculations so far have appeared for energies higher than that owing to difficulties in the divergence of the numerical integration. However, the relativistic hydrogenic wave function indeed produces part of the necessary correction at $\eta \lesssim 0.01$, as indicated by many authors.[28,14,3] We show, in Fig. 9, that the cross-over points of $\sigma_{L_1}(E)$ and $\sigma_{L_2}(E)$, and of $\sigma_{L_1}(E)$ and $\sigma_{L_3}(E)$, are much closer to the predictions of the relativistic PWBA than that of the nonrelativistic PWBA.

Use of the Hartree-Fock-Slater wave functions may also produce calculational effects which are sizable for L-shell electrons, especially in the region where there is a node.[29] From a comparison of hydrogenic and Hartree-Fock $l=1$ radial eigenfunctions for mercury,[29] it is seen that the Hartree-Fock-Slater wave functions do tend to have the node at a higher momentum. In order to investigate these two effects, we compared the ratios $\sigma_{L_1}/\sigma_{L_2}$ taken from our data, to those predicted by PWBA. The Coulomb-deflection effect and binding effect, which are significant at the low energies as discussed at the beginning of this section, should be eliminated, since they affect each subshell in a similar manner.[30] Figures 8(a)–8(c) show the energy dependence of these ratios for Ta, Au, and Bi, respectively. The val-

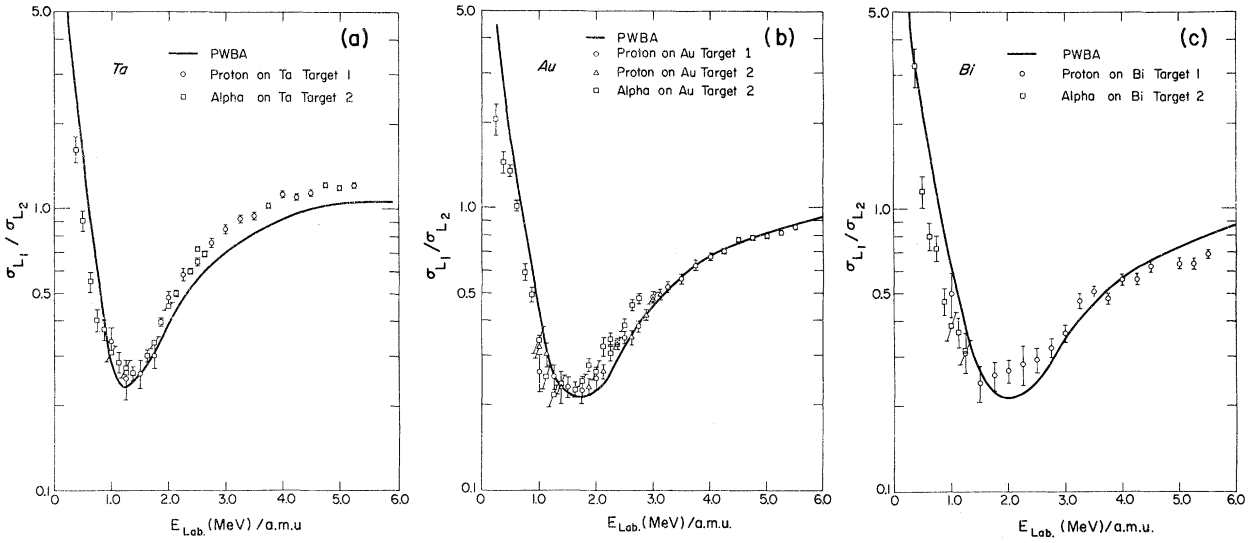

FIG. 8. Cross-section ratio $\sigma_{L_1}/\sigma_{L_2}$ for (a) Ta, (b) Au, and (c) Bi.

leys of these ratios reflect the location of the node in the momentum distribution of the $2s_{1/2}$ electrons. Again these ratios are qualitatively described by nonrelativistic PWBA quite well. The gradual shift of the position of the valley predicted by nonrelativistic PWBA toward energies higher than the experimental position, as one goes from tantalum to bismuth, may be due to a stronger Z dependence of the node position in the hydrogenic wave functions than in the actual atomic wave functions. A Hartree-Fock-Slater type of calculation thus is very important to undertake at this point to clarify which effect dominates the shift of the valley of the $\sigma_{L_1}/\sigma_{L_2}$ ratios.

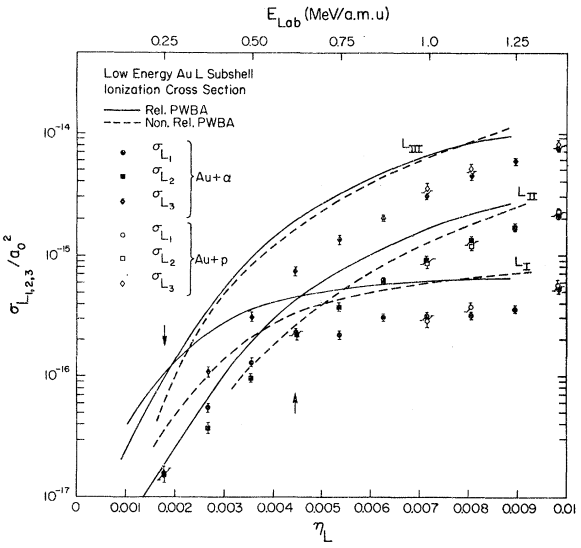

FIG. 9. Low-energy Au cross sections compared with nonrelativistic and relativistic PWBA calculations.

This Hartree-Fock-Slater correction is expected to have a negligibly small effect on the observations of σ_{L_2} and σ_{L_3}; wave functions having no nodes, such as those of $2p_{1/2}$ and $2p_{3/2}$, seem to be relatively well described, for present purposes,

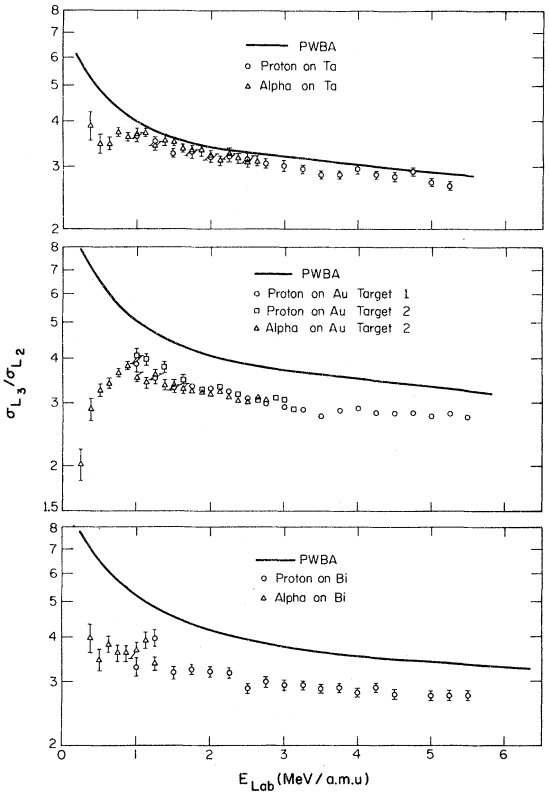

FIG. 10. Ratio $\sigma_{L_3}/\sigma_{L_2}$ for Ta, Au, and Bi.

by hydrogenic wave functions. One expects that the energy dependence of the $\sigma_{L_3}/\sigma_{L_2}$ ratios can thus be predicted much better than the $\sigma_{L_1}/\sigma_{L_2}$ ratios by PWBA. Figure 10 shows these ratios. The vertical uniform displacement between data and theory may be due partly to the uncertain absolute values of the atomic parameters such as ω's and F's involved in the data analysis. The relativistic correction also tends to lower the theoretical curve.[3,28] It can also be seen, from Fig. 9, that relatively larger corrections must be made for σ_{L_2} than for σ_{L_3} owing to the relativistic effect at $\eta_L \lesssim 0.01$, which will move the theoretical calculation of the $\sigma_{L_3}/\sigma_{L_2}$ ratio downwards toward the data. The dramatic drop of the $\sigma_{L_3}/\sigma_{L_2}$ ratio in the α data at lower energies was first observed by Datz *et al.*,[3] who measured $\sigma_{L_3}/\sigma_{L_2}$ for Au. However, a corresponding steep drop in the α data in Ta and Bi is not observed. This phenomenon has been explored in some detail and the results are published elsewhere.[31]

V. CONCLUSIONS

The features of L-subshell ionization of a heavy atom by a light ion can generally be described through a Coulomb interaction in the framework of PWBA. Through a study of $2s_{1/2}$ ionization, finer details of the ionization process are revealed. These details suggest the necessity of further calculations involving more sophisticated wave functions, such as the Hartree-Fock-Slater type, which could contribute a sizable effect in the heavy elements, along with relativistic corrections. A nonrelativistic PWBA calculation using Hartree-Fock-Slater wave functions to indicate the quantitative shift of the valley of the $\sigma_{L_1}/\sigma_{L_2}$ ratio would be instructive and illuminate the usage of light ions as a probe to investigate the characteristic of the electrons in the deep shells of the atom.

The features of the $\sigma_{L_3}/\sigma_{L_2}$ ratio at low energies of alpha-particle bombardment are also very interesting, and may end up producing new physical insight. However, more experimental information is needed before final conclusions can be made. Such information could include detailed high-resolution L x-ray spectra (to be sure that additional or "satellite" peaks are not violating the data-reduction assumptions made in the present study), and energy-dependence measurements on atoms around the closure of other s subshells, such as $5s$ (to see if the apparent dependence persists). Such studies are presently underway.

---

†Work supported in part by the NSF.
*Supported in part by O.S.U. Graduate School Research Grant.

[1]G. A. Bissinger, S. M. Shafroth, and A. W. Waltner, Phys. Rev. A 5, 2046 (1972).
[2]L. M. Winters, J. R. MacDonald, M. D. Brown, L. D. Ellsworth, and T. Chiao, Phys. Rev. A 7, 1276 (1973).
[3]S. Datz, J. L. Duggan, L. C. Feldman, E. Laegsgaard, and J. U. Andersen, Phys. Rev. A 9, 1972 (1974).
[4]E. Merzbacher and H. W. Lewis, *Encyclopedia of Physics*, edited by S. Flügge (Springer-Verlag, Berlin, 1958), Vol. 34, p. 166.
[5]G. S. Khandelwal and E. Merzbacher, Phys. Rev. 144, 348 (1966).
[6]J. Bang and J. M. Hansteen, K. Dan. Vidensk. Selsk. Mat.-Fys. Medd. 31, No. 13 (1959).
[7]J. M. Hansteen and O. P. Mosebekk, Z. Phys. 234, 281 (1970).
[8]J. D. Garica, Phys. Rev. A 1, 280 (1970).
[9]J. A. Hansen, Phys. Rev. A 8, 822 (1973).
[10]G. J. Basbas, thesis (University of North Carolina, Chapel Hill, 1968) (unpublished).
[11]V. S. Senashenko, V. S. Nikolaev, and V. Yu. Shafer, Phys. Lett. 31A, 565 (1970).
[12]R. L. Watson, C. W. Lewis, and J. B. Natowitz, Nucl. Phys. A 154, 561 (1970).
[13]N. Tsoupas, Ph.D. thesis (Ohio State University, 1974) (unpublished).
[14]G. A. Bissinger, A. B. Baskin, B.-H. Choi, and S. M. Shafroth, in *Proceedings of the International Conference on Inner-Shell Ionization Phenomena* (U.S. A.E.C. pub. CONF-720404, Oak Ridge, Tenn., 1972), Vol. 2, p. 1102.
[15]F. Abrath and Tom J. Gray, Phys. Rev. A 9, 682 (1974).
[16]J. H. Scofield, Phys. Rev. 179, 9 (1969).
[17]D. W. Nix, J. C. McGeorge, and R. W. Fink, Phys. Lett. 46A, 205 (1973).
[18]J. H. McGrary, L. V. Singman, L. H. Ziegler, L. D. Looney, C. M. Edmonds, and C. E. Harris, Phys. Rev. A 5, 1587 (1972).
[19]S. I. Salem, D. C. Clark, and R. T. Tsutsui, Phys. Rev. A 5, 2390 (1972).
[20]Walter Bambynek, B. Crasemann, R. W. Fink, H.-U. Freund, H. Mark, C. D. Swift, R. E. Price, and P. V. Rao, Rev. Mod. Phys. 44, 716 (1972).
[21]C. W. Lewis, R. L. Watson, and J. B. Natowitz, Phys. Rev. A 5, 1773 (1972).
[22]E. M. Bernstein and H. W. Lewis, Phys. Rev. 95, 83 (1954).
[23]H. Fraunfelder and R. M. Steffen, in *Alpha-, Beta-, and Gamma-Ray Spectroscopy*, edited by K. Siegbahn (North-Holland, Amsterdam, 1965), Vol. 2, p. 997.
[24]C. N. Chang, Ph.D. thesis (Ohio State University, 1974) (unpublished).
[25]B.-H. Choi, E. Merzbacher, and G. S. Khandelwal, At. Data 5, 291 (1973).
[26]G.Basbas, W. Brandt, and R. Laubert, Phys. Rev. A 7, 983 (1973).
[27]E. Merzbacher, in *Proceedings of the International Conference on Inner-Shell Ionization Phenomena* (U.S. A.E.C. pub. CONF-720404, Oak Ridge, Tenn., 1972), Vol. 2, p. 915.

[28]B. Choi, Phys. Rev. A 4, 1002 (1971).
[29]M. H. Chen, B. Crasemann, and V. O. Kostroun, Phys. Rev. A 4, 1 (1971).
[30]Following the formula given by W. Brandt and G. Lapicki, Phys. Rev. A 10, 474 (1974), we find that the general theoretical shape of $\sigma_{L_1}/\sigma_{L_2}$ of PWBA with binding and Coulomb deflection corrections is little different from the PWBA without these two corrections; particularly, the valley positions of $\sigma_{L_1}/\sigma_{L_2}$ are the same with and without binding and Coulomb deflection corrections.
[31]C. N. Chang, J. F. Morgan, and S. L. Blatt, Phys. Lett. 49A, 365 (1974).